applied sciences

*Article*

# An Investigation of Quasi-Static Compression and Shock Responses under a Pneumatic Exciter on Brittle Truss Lattice Structures Fabricated with a Vat Photopolymer Resin

**Patchayaporn Doungkom, Thira Jearsiripongkul and Krit Jiamjiroch ***

Department of Mechanical Engineering, Faculty of Engineering, Thammasat School of Engineering, Thammasat University, Pathumthani 12121, Thailand; jthira@engr.tu.ac.th (T.J.)
* Correspondence: jkrit@engr.tu.ac.th

**Featured Application: shock isolation, insert structure for non-structural aviation or insert structure for biomedical applications.**

**Abstract:** Shock attenuation is a significant aspect of shockproof design. The aim of this study is to explore the use of lattice structures for shock isolation applications. Five lattice structures were fabricated using photopolymer resin and subjected to quasi-static compression tests under a universal testing machine and shock response tests under a pneumatic exciter. The quasi-static compression tests provided preliminary data on the lattice structure's collapse modes, stress, strain, and energy absorption. The shock test results revealed that the responses from the lattice structures were complex convolutions of the frequency. Moreover, the collapsed mode under the compression experiment did not guarantee the same outcome as in the shock impulse experiment. Amongst the lattice structures, the face-centred cubic with cubic perimeter (FCC + CP) structure exhibited the poorest shock isolation properties, with an ability to absorb only approximately one-third of the shock compared to solid structures. On the other hand, the body-centred cubic with cubic perimeter (BCC + CP) structure showed the highest impulse response with average shock transmissibility, making it a viable option for applications requiring shock insulation. However, it should be noted that this data may only be applicable for high acceleration with low degrees of force, less than 300 N.

**Keywords:** lattice structure; quasi-static; shock response; pneumatic shock; transmissibility

check for updates

**Citation:** Doungkom, P.; Jearsiripongkul, T.; Jiamjiroch, K. An Investigation of Quasi-Static Compression and Shock Responses under a Pneumatic Exciter on Brittle Truss Lattice Structures Fabricated with a Vat Photopolymer Resin. *Appl. Sci.* **2023**, *13*, 6087. https://doi.org/10.3390/app13106087

Academic Editors: Carlos Miguel Santos Vicente and Marco Leite

Received: 4 March 2023
Revised: 6 May 2023
Accepted: 10 May 2023
Published: 16 May 2023

**Copyright:** © 2023 by the authors. Licensee MDPI, Basel, Switzerland. This article is an open access article distributed under the terms and conditions of the Creative Commons Attribution (CC BY) license (https://creativecommons.org/licenses/by/4.0/).

## 1. Introduction

Lattice structures hold great appeal in a diverse range of lightweight constructions [1], particularly those of vehicles and aircraft [2,3]. They are well-suited to their intended purposes due to their inherently light mass and sufficiently high strength-to-weight ratio [4]. Moreover, they have sparked the curiosity of numerous scientific minds in their bid to comprehend their structural intricacies and garnered immense attention from various industries, which regard them as an integral facet of their operations [5]. Given the exquisitely sophisticated nature of these structures, the lattice arrangement has the potential to make a significant difference to their original material, resulting in many possibilities in engineering design. Notably, the solid body has been removed, reducing the ultimate strength [6]. Whilst it is possible that the structural integrity of this construction may be compromised to some degree, it has the potential to augment the strength-to-weight ratio in favourable circumstances [7,8]. Consequently, optimising this structure using computres by finite element model (FEM) before deploying it for appropriate applications is crucial [9–11].

It is noteworthy that this process has the potential to enhance the noticeable attributes of most materials, given that lattice structures are naturally weight-reducing frameworks, as it contends many air voids [7]. Nonetheless, in spite of this potential drawback, the substandard sound transmission characteristics of such air pockets render them a feasible alternative for employment in architectural designs devised for soundproofing objectives. [12,13]. In medicine, lattice structures possess the potential to function as a scaffold for a diverse array of implants, bone grafts, and joint replacements [14]. Moreover, in contrast to their bulky, weighty counterparts found in several earlier iterations, these frameworks are endowed with reduced stiffness, rendering them far more comfortable for recipients of transplants [15]. Correspondingly, various efforts have been made in lightweight applications to incorporate these lattice structures in both structural and non-structural components of vehicles and aircraft [16], owing to their ability to curtail fuel consumption by providing a weight-reducing framework.

Current endeavours are introducing lattice structures for shock absorption in passenger cars [17]. In addition, computer-aided design simulations demonstrate that closed cellular networks exhibit immense potential as a promising technology, as they possess superior energy-absorbing capabilities [10]. Regarding the FMVSS 208 [18], frontal crash test, vehicles must be subjected to a collision with a rigid barrier at a velocity of 35 mph or (60 km$\cdot$s$^{-1}$), resulting in an impulse value of roughly 10,000 Nm$\cdot$s$^{-2}$. For smaller vehicles, such as motorcycles, SAE J211 [19] outlines an array of dynamic requisites for various types of impact assessments. In the case of motorcycle helmets, the standard mandates that the head form employed in the test weighs 5 kg and must be equipped with an impact velocity ranging from 4.5 to 7.5 m$\cdot$s$^{-1}$. Additionally, the CPSC [20] stipulates that bicycle helmets should protect a 5 kg object with an acceleration of 300 g.

Under quasi-static compressive loading, the type of deformation observed in materials is dependent on their characteristics. Stretching-dominated and bending-dominated deformations have been identified in metallic alloys [21–23] and plastics [24–27]. Studies have indicated conflicting collapsed modes that may have implications for material selection and manufacturing processes [23]. Two BCC lattices with the exact dimensions were prepared using traditional casting and SLM techniques. Although both samples are based on the same material, they had different responses due to the grain of the samples [23]. Research conducted through quasi-static compression testing on lattice structures has revealed a sequential layer-by-layer collapse at a similar stress level, as documented in existing literature [22,28]. However, variations in the preparation techniques of identical architecture and material using SLM and casting may result in differences in the collapsed mode [23]. A Gibson-Ashby model [29] and Maxwell's number [30] are the models that may provide a rudimentary prediction for the mode of failure of a lattice structure.

Additionally, tensile testing of SLM structures has shown higher ultimate strength than those produced through casting. Scanning Electron Microscope (SEM) images indicate that samples from SLM printers have more controllable dimensions but may have coarser grains than those made through casting. Even well-prepared lattice structure specimens with identical materials may exhibit different deformation modes. Hence, information on a lattice's structure or material cannot be considered an adequate tool for predicting the collapsed mode since their behaviour is dissimilar [23]. Topological modifications to many lattice structures, such as the introduction of a "Z" column to each unit cell (e.g., BCC and BCCZ) [25,27], may increase the rigidity and strength of the structure [31]. For example, a polymer lattice structure with topological structures like BCCZ, DiamondZ, and PyramidZ has been observed to exhibit higher strength than its original structure [27].

The phenomena of shock and impulse show notable similarities, yet distinct specifications exist between the two. Shock refers to the collision of a force, which is typically excited through solid or non-solid compactors, such as sound waves, with objects. In contrast, impulse pertains to the collision between two solid objects. Both shock and impulse are characterised by sudden excitation between an exciter and a target, and such collisions may occur at either intermediate or high strain rates [28]. Although shock and impulse are distinct phenomena, they are often associated with one another. Shock has a unit of measurement as acceleration in (g) and frequency (f) in (Hz or rad$\cdot$s$^{-1}$) while impulse is a change of momentum that can measure in (N$\cdot$s or kg m$\cdot$s$^{-1}$).

There are many methods for conducting shock measurements, with the most prevalent techniques being Charpy impact, pneumatic exciter, and Hopkinson bar tests [32–34]. Shock experiments can be performed using a variety of exciters, such as the conventional Charpy impact test [35]. However, this method may lack sensitivity as it does not discern different responses between BCC and BCCZ structures while identifying a higher elastic modulus in Gyroid structures [35]. One study examining high-strain rate testing focused on the macroscopic shock response obtained from elastically isotropic metallic structures with orthogonal plates and a relative density ranging from 0.225 to 0.229. In this research, both structures were made of 316 L stainless steel using a powder-bed fusion additive manufacturing approach. Although this investigation employed orthogonal plates, it provided valuable data for quasi-static and high-dynamic impact testing using a Hopkinson bar. In comparison to the quasi-static test, the maximum stress observed in high-strain rate experiments may decrease due to premature fracture [28]. The Hopkinson split bar, another piece of equipment for both tensile and compressive testing, can generate acceleration up to an ultra-high shock of 10,000 g [36]. This exciter, increasingly utilised for high to ultra-high shock acceleration, has become a standard in acceleration calibration and mechanical testing [37]. The responses of various lattice structures during this test exhibit signs of viscoelasticity, as different travel wave velocities are observed. Under these testing conditions, the complex modulus is dependent on the impact frequency [38].

Most of the work done with the high strain rate or "shock" were mostly alloy or metal structures; the polymer is less well-known in this area6 as it has a less strong impaction strength and can be used in vehicle bumper applications [39,40]. Moreover. there has not been much research into the shock area, but one piece of research was similar: some of the details focused on the polymers BCC and ECC (edge-centered cubic) lattice structures [41]. Despite the metallic shock impulse study, the BCC and ECC polymer lattices, prepared by an FDM-3D printer, were investigated, using a dynamic shock absorption machine. The dynamic shock absorption machine is a kind of low shock impulse machine that uses a drop weight with a variation of the porosity per centage between 65.4 to 83.5. The BCC and ECC structure had a 12 mm controllable cube cell size, but there were three sizes of the studs' diameters (2.4 mm, 2.8 mm and 3.2 mm). The shock impulse can be used as one of the indicators, and it was concluded that the BCC structure with a stud diameter of 2.8 mm produced the best shock absorption. Regarding the different structures, they might not necessarily behave the same. They were also repeatedly tested with an edge-centered cubic lattice structure, and the smallest stud size showed better shock absorbance [41].

The higher strain rate of a high shock acceleration of several lattice structures has been studied, using a Hopkinson bar [42], and there was a signal response that changed tremulously between the medium and high strain rates when the strain rate was increased [43]. Rankine-Hugoniot is interfacial between low and high pressure that happens under shock [34], which is necessary to be observed by high-speed camera [42]. The study was done with experiments and numerical techniques, concluding that three lattice structures were directly impacted by up to approximately 70 m/s. Also, it seems that all lattice structures suffered a catastrophic failure with the direct impact; the higher the excited velocity shown, the more sign of the convolution curve. The stress showed a positive effect with a relative density, but the energy absorption also had a certain extent correlation with a relative density [42]. In general, transmissibility (T, [-]) refers to the ability of a material to attenuate shock during impulse testing or isolate vibration in response to force vibration. It can be defined as the ratio between the resulting force and the input or excited force. Transmissibility can be viewed as an indicator of efficiency in vibration isolation for all types of materials, including lattice structures. [44].

Although several researchers have investigated the mechanical properties of lattice structures, most of them have been quasi-static. From the literature survey, it appears that no investigations have thus far been conducted concerning the dynamic phenomena of lattice structures in the context of pneumatic shock exciters. Nonetheless, it is of utmost importance to perform preliminary examinations under quasi-static conditions in order to obtain fundamental knowledge. This particular investigation not only offers crucial mechanical properties and collapse modalities for quasi-static assessments, but it also aids in identifying suitable lattice structures for shock impulse utilisation. The findings of this scholarly pursuit are anticipated to considerably enhance the comprehension of lattice structures' shock response behaviour, thereby facilitating more informed decision-making within engineering applications.

## 2. Materials and Methods

Most of the numbers presented in this article are reported with an average ± repeatability, using the Guide to the Expression of Uncertainty in Measurement (GUM) [45]; Nevertheless, the numerical value resulting from the quasi-static compressive test is exclusively reported as an average number as only three specimens were used in the test. The information regarding linear shock impulse experiments was collected based on at least four peaks establishing the multiple impactions. Finally, the terminology used throughout the manuscript adheres predominantly to ISO/ASTM 52900 [46].

### *2.1. Specimen*

The five lattice types of the sandwich structures, as referenced in the literature [47], were fabricated by a vat photopolymer printer (Wanho GR-1) with light-sensitive resin. Based on ASTM D1621 [48], the dimensions of the quasi-static compression test are shown in Figure 1i. Regarding toe adaption, the dimensions of the lattice structure, which can work with a shock impulse machine, as BS- ISO 16063:2015 [34] are shown in Figure 1ii. The sandwich structure of the specimens was 40 × 40 × 60 mm with a lattice control cell size of 4 × 4 × 4 mm, which was used for the compression in this experiment. As there was a limitation of spacing of the impact rig, the smaller sandwich structure of the lattice was printed with a diameter of 12 mm, as shown in Figure 1. This 3D printer can print a specimen with a minimum stud size of 0.5 mm. Because the mechanical properties could change upon the difference post-cured time [49]. To attain the highest level of curing, it is imperative to observe that specimens obtained from light-sensitive resin necessitate undergoing a post-curing process of approximately five minutes, followed by exposure to UV light for six hours, before being retained in a dark environment.

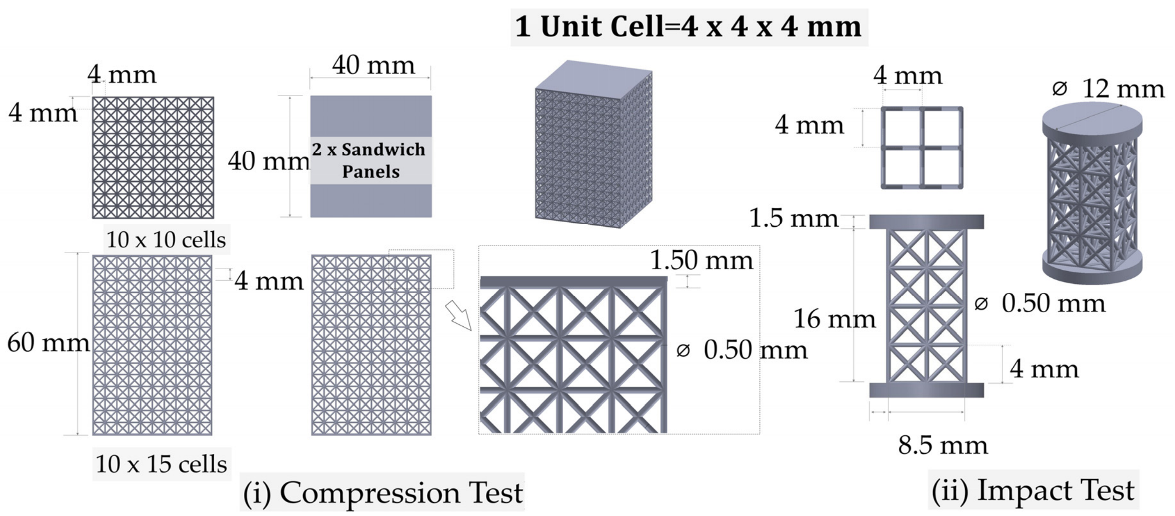


**Figure 1.** The details of the sample for (**i**) Quasi-statistic compression and (**ii**) shock impulse testing.

There are five lattice structures, as shown in Table 1, which are the cubic perimeter (CP), body centre cubic (BCC), face centre cubic (FCC), it can be stated that the face-centered cubic configuration comprises of the connections located at each of the eight corner positions, as well as at the center of each of the six faces. On the other hand, the body-centered cubic configuration consists of the connections situated at each of the eight corner positions, in addition to another atom located at the centre of the cube. The combination between these two basic structures with the cubic perimeter are BCC + CP and FCC + CP. All samples were fabricated at the identical cell size (4 × 4 × 4 mm) with the same stud diameter of 0.5 mm, as previously mentioned (see Figure 1). These samples were subjected to the quasi-static test (Section 2.3) and shock impulse test (Section 2.4).

**Table 1.** The Lattice structure for compression testing and impact testing.

| Lattice | Unit Cell | 16 Unit Cell | 1500 Unit Cell | Relative Density |
|---|---|---|---|---|
| CP | 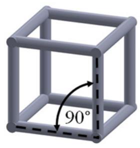  | 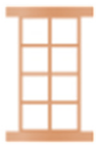 | 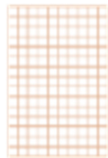 | 0.066 |
| BCC |   | 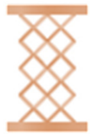 | 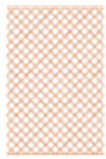 | 0.121 |
| FCC | 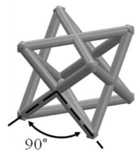  | 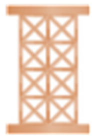 |  | 0.121 |
| BCC + CP | 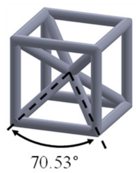  | 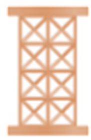 | 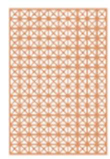 | 0.136 |
| FCC + CP | 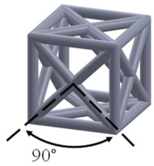  | 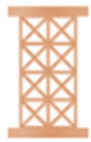 | 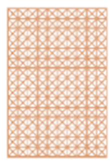 | 0.158 |
| Solid | 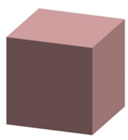 |  |  | 1.0000 |

Remark: Relative density, also known as specific gravity, is defined as the ratio of the density of a substance ($\rho^*$) to the density of a reference substance ($\rho_s$).

### *2.2. ANOVA Test*

Decision-making is one of the other extents in this research; the confidence level or alpha ($\alpha$) calculation with Analysis of Variance (ANOVA) is becoming a scientific tool because it can indicate the significant effects of the responses on the desirable factors with the null hypothesis ($H_0$) needing to be set before the experiment begins. In the case of acceptance of the null hypothesis at a 95 per cent of confidence level ($p$ value > 0.05), there is no different effect between the testing parameter or between the testing groups; however, if the null hypothesis is rejected with the acceptance of an alternative hypothesis, the $p$ value is less than 0.05 and to avoid the repeated signal of the alternative hypothesis acceptation with "the significant difference at the 95 per cent of confidence level" that may indicate the super subscript symbol of "†" at the end of the sentence but if the null hypothesis is acceptation, that may show the super subscript symbol of "‡". The hypothesis can be tested by the R Project for Statistical Computing [50], a freeware project originally from Bell Laboratories. This software has the capability not only to analyse the data in general statistics but also can be used to analyse in both ANOVA and Post hypotheses testing [51]. The simple null hypotheses were established for the quantitative response with the compressive test and shock impulse testing. In null hypotheses, there were insignificant effects on the responses of many reactions operating with the different lattice structures under both the quasi-static compression testing and shock impulse testing methods and no significantly different effects on the responses of mechanical properties at the difference excited force levels.

### 2.3. Quasi Static Compressive Test

According to the ASTM D1621 [48]: Standard Test Method for Compressive Properties of Rigid Cellular Plastics, guidelines, all the specimens were subjected to compressive load testing. The test was conducted with a preload on a Universal Testing Machine (UTM): Instron 5969, equipped with a 50 kN load cell for lattice structures and 1000 kN for a solid plastic block. The strain rate was kept constant at 2.25 $mm \cdot min^{-1}$, in accordance with the ASTM D1621. The force-extension curves were analyzed and transformed into stress ($\sigma$, $N \cdot m^{-2}$) and strain ($\varepsilon$, [-]) using the procedures outlined in Appendix A of ASTM D695-02 [52], Additionally, stress was estimated from the experimental results by calculating the ratio between force and the overall cross-sectional area of the specimens. An elastic modulus (E, Pa) was also calculated by dividing the stress by the strain for all specimens [48].

To obtain the results for lattice structures, the Gibson-Ashby model (represented by Equation (1) was used. This method involves plotting the relative density ($\rho^*/\rho_s$) against the normalised mechanical properties, with respect to the solid property. The SONY RX100 IV camera was used to capture the impressions during the compressive test. The stress and strain curve yielded important information about yield stress, stress at break, and Young's modulus of the specimens, which could be a function of the normalisation of density ($\rho^*/\rho_s$) or relative density. Additionally, a series of deformation impressions was expected to reveal significant patterns of collapsing, and the collapsed failure mode may depend on the "n" coefficient, which is a collapsing mode coefficient [53].

$$\rho^*/\rho_s \propto (x^*/x_s)^n \tag{1}$$

Not only were those normalised mechanical properties obtained with a quasi-static experiment, but energy absorption per volume (W, $J \cdot kg^{-1}$) was another response that was estimated by integrating a force of up to 65 per cent of the strain rate in this study.

### 2.4. Shock Impulse Test

The instruments were considered an essential part of this study; an in-house pneumatic exciter was the main equipment used for this section; this rig is originally aimed for shock calibration, as mentioned in the literature [54] (see Figure 2), according to BS-ISO 16063:2015 [34]. The pressure is effectively regulated by a closed-loop control system, which is accompanied by a fire command on the Human-Machine Interface (HMI) developed with LabVIEW™ version 2020. The machine fingers were used to mount both of the lattice specimens, and upon a specific force, the specimen was impacted with an anvil. The impact data were then measured using an Endevco® accelerometer (2270 M8) with a sensitivity of (S = 2.06 $pC \cdot g^{-1}$) [43] with a charge amplifier system (2771 C) with Gain (G = 0.1 $mV \cdot pC^{-1}$) then all the data were recorded at high-speed with a maximum speed rate of 1.25 $MS \cdot s^{-1}$ by DAQ National Instrument NI-PXIe-4480 card, but the record speed rate used in this experiment was 512 $kS \cdot s^{-1}$ in order to reduce a redundant data. After that, all of the data from the accelerometer were converted from the voltage ($V_s$, V) into acceleration (a) based on (Equation (2)) [33].

$$|\mathbf{a}| = G \times V_s/S \tag{2}$$

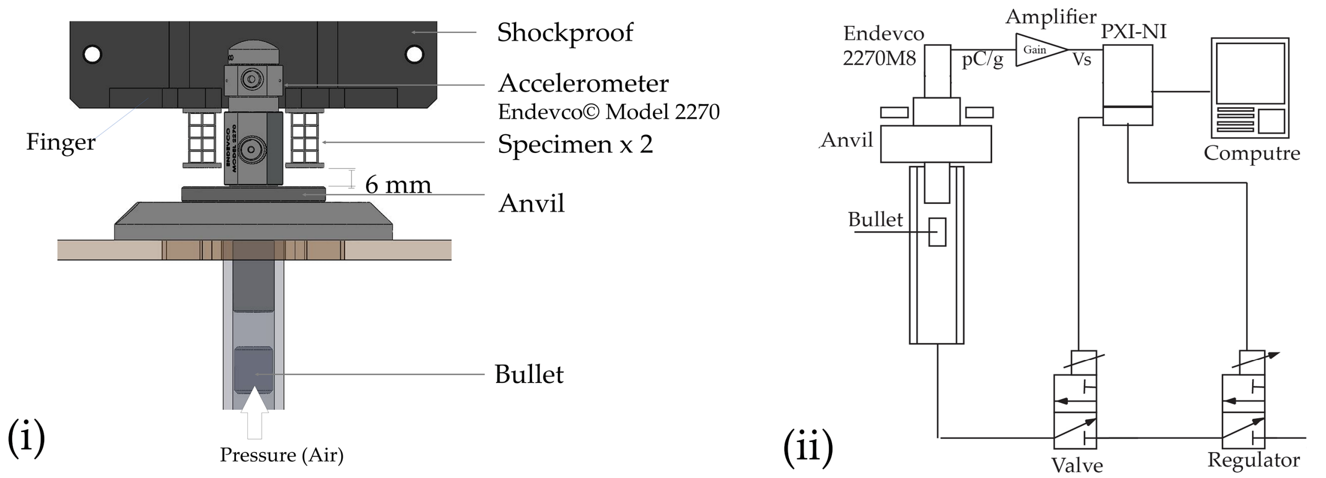


**Figure 2.** Schematic diagram of a shock impulse generator based on the BS-ISO 16063:2015. (**i**) the diagram of specimen setup with the finger of the rig (**ii**) schematic diagram of the rig.

The prevalent units of an accelerometer (**a**) utilised are (m/s$^2$) or the force of gravity (g), estimated at roughly 9.81 m/s$^2$. This experiment was performed by mounting two specimens on the finger of the test rig, as shown in Figure 2. All of the shock impulse specimens are again referred with an input force (**F**, N). Reference impulse force is an impulse (**P**, N·s) obtained from testing without the mount samples on the finger of an acceleration test rig (see Equation (3)).

$$\mathbf{P}(\mathrm{t}) = \int \mathbf{F}(\mathrm{t})\ \mathrm{dt} = \mathrm{m} \int \mathbf{a}(\mathrm{t})\ \mathrm{dt} \tag{3}$$

The linear impulse in this study was generally based on the instability of an acceleration in (g) over an impulse time (τ, ms) being transformed into a force over impulse time. This linear impulse represents the area under the curve between force over time, while acceleration is necessary to be estimated, using the following BS-ISO 16063:2015. According to this standard, an impulse curve would tread with a half-sine pulse, and the impulse time could be estimated by offsetting 10 per cent of a peak signal from the reference baseline. Not only did the results improve with a baseline correction, but it was necessary to perform pass filtering by the order 4 of a Butterworth filter.

In this case, the variation of an acceleration, (**a**, g) would be affected by the fluctuating forces. (**F**, N). Because the acceleration in a time domain was a half-sine, this could, over time, result in the response of the force also becoming a half-sine. Hence, the integration of the area under the curve, between F and t, could yield a linear impulse. The half-sine pulse may either plot in a function of sine as shown in (Equation (4)).

$$|\mathbf{a}| = |\mathbf{a_{max}}|\ \sin(\pi \mathrm{t}/\tau) \tag{4}$$

where as $\mathbf{a_{max}}$ represents the maximum amplitude of the acceleration and τ is impulse time in (milli second, ms). The half-sine pulse may apply under the assumption of critical damping, which was found only in the single pulse with a single impact. Figure 2. shows the picture of the experiment rig. This rig is generally designed for a shock calibration and can generate a shock acceleration that can be converted into a very accurate linear impulse. There are two specimen mouths on the finger of the rig. After the pressure is provided, the anvil will move upward and collide with the specimen.

## 3. Results and Discussion

As mentioned earlier (Section 2), all of the results shown with have repeatability. This paper is separated into two discrete experiments with similar lattice structures. Section 3.1 explains and discusses the results of the quasi-static compression testing, and Section 3.2

offers the empirical modelling based on Gibson-Ashby model [29]. Lastly, the shock responses were tested with the different lattice structures shown in Section 3.3.

### 3.1. Quasi-Static Compression Testing

The series of collapsing photographs found in the quasi-static compression test are shown in Figure 3. The five lattice samples are the CP, BCC, FCC, BCC + CP, FCC + CP and the solid samples were subjected to compressive testing. It can be seen that the CP sample was collapsing layer-by-layer. This failure mode was reported and recognised as a "sequential local collapse". More specifically, the CP structure collapse did not break on the column, but its column was folding from side to side [14]. This incidence may indicate the presence of an uncontrolled element on the column, enabling the smooth transition of the upper layout from either a leftward or rightward direction [55]. The findings from the Finite Element Method (FEM) analysis of the CP framework in the literature revealed that the utmost strain occurs predominantly along the vertical edge of the CP. Moreover, it was observed that the strain is dispersed and mitigated at the bottom of the units. [56] that could be lead to result in a "sequential local collapse". The collapse of the BCC structure was due to bending, while the others were stretching-dominated, and it could be evidenced that all of the collapsing modes were independent of the Maxwell's number. This could be caused by the stress distribution from the FEA of the BCC structure occurring as the two pyramids joined at the top [21]. The FCC and FCC + CP were likely fractured with a layer-by-layer collapse, the same as the CP structure, but their fracture was 45 degrees and shifted to the side of the sample instead (see Figure 4). It seems that by introducing a Z column, the topological lattice structure could closely introduce the same shear stress level.

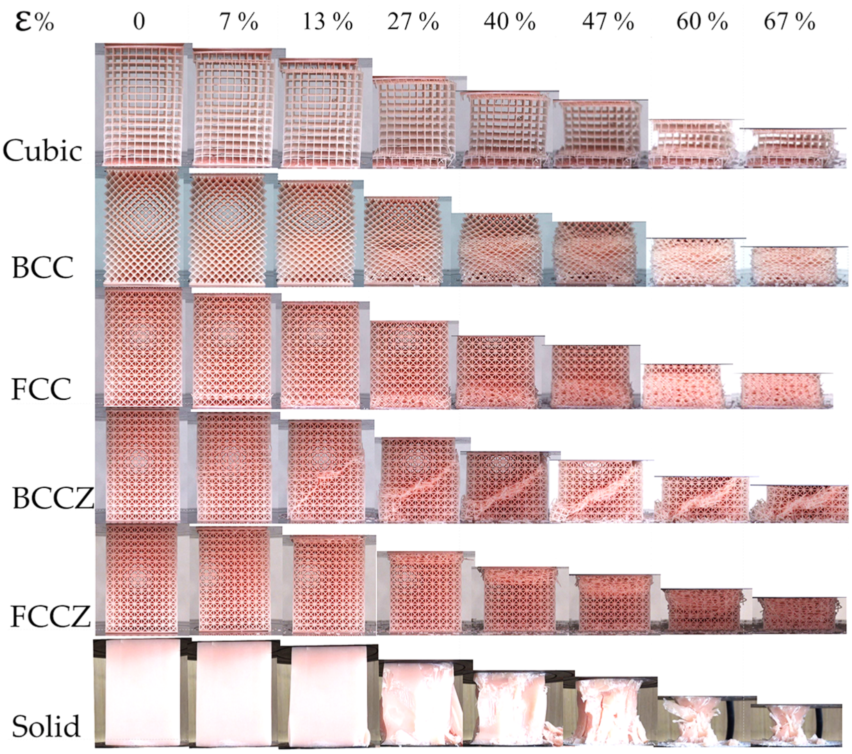


**Figure 3.** The impression of the quasi-static compression of the lattice structure and a solid sample obtained from a vet uv curable photopolymer 3D printer. This complication shows samples with the CP combination of BCC + CP and FCC + CP had complications.

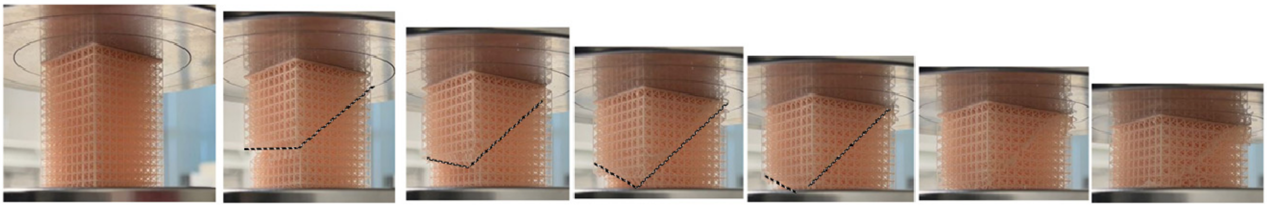

**Figure 4.** The angle views of the failure mode found in the FCC + CP structure show the stretching collapsed mode. Once, this FCC + CP sample was subjected to uniaxial compression testing.

The stress-strain curves obtained from a uniaxial compression test conducted on the CP structure are presented in Figure 5i. The CP structure exhibited a layer-by-layer collapse, which serves as a reference for all of the lattice structures. Its average yield strength was found to be 181.4 $\pm$ 0.1 kN$\cdot$mm$^{-2}$, which translates to a 99.5% reduction from its solid material. While the CP structure had the least strength among the structures tested, but it remains a good representative of a lattice structure as it retains a layer-collapsing provision. In contrast, the BCC structure may have a different failure mode (bending-dominated), resulting in a notable plateau or plastic deformation in elastomer plastic. The compressive stress did not vary significantly ($p$ = 0.06) between 14.7 and 48.9 per cent of the strain rate[‡], and this plateau region in the BCC structure would exhibit similar results to that of the CP[‡]. Although the results show good agreement between the two structures in the plateau region, more experiments are required to confirm this statistically.

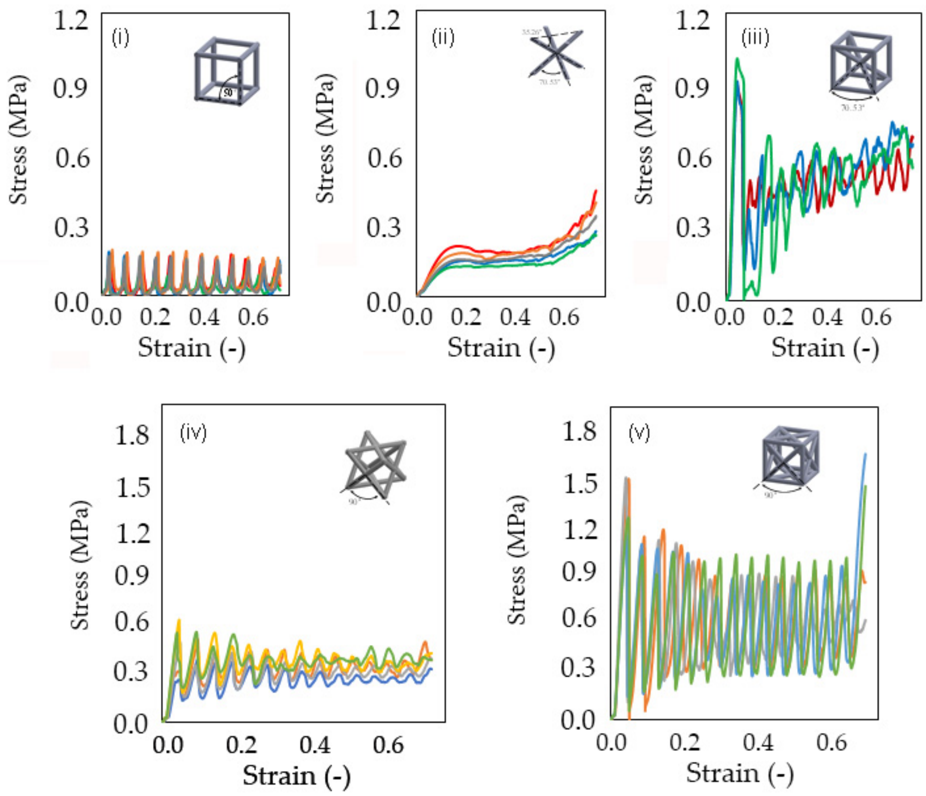


**Figure 5.** The cohort of stress-strain curves of (**i**) Cubic Perimeter (CP), (**ii**) BCC, (**iii**) FCC (**iv**) BCC + CP and (**v**) BCC + CP lattice structures from a quasi-static compression test based on ASTM D1621, The distinct colors indicate different reflections of the same structure. The depicted images illustrate a high degree of repeatability in various types of lattice structures when subjected to quasi-static loads.

Many articles have been written regarding BCC lattice structures; however, it should be noted that the occurrence of the plateau region on this type of structure is not always guaranteed. Furthermore, it has been observed that the BCC metal structures described in the reference [5] do not exhibit a significant plateau region and tend to collapse under a stretching-dominated structure [5]. On the other hand, polymer lattices fabricated with polymer-cured resin have been found to collapse under a bending-dominated structure [25]. It is evident from the literature that the fabrication technique, in addition to architecture and material, plays a crucial role in determining the mode of collapse [29]. Thus, individual structure architecture might not offer enough data to determine the exact collapsed mode of individual lattice structures, but the combination of at least three parameters: the lattice architecture, material in-use and manufacturing technique, could be the essential information for making a prediction.

In this test matrix, all the lattices, constructed with the same material and technique, show that stress over strain curves for individual structures could offer the same repeated result (see Figure 5). The cohort of the stress-strain curves in Figure 5, indicates a sequence of layer collapse, consistent with what has been previously documented [5]. However, it would not be rational to represent these findings on a single graph, as the stress-strain curve of the BCC + CP exhibits a random breakage of collapsing peaks subsequent to the ultimate strength. Figure 6 presents a graphical representation of stress-strain curves for various lattice structures, with reference to the CP structure. A strong correspondence is observed between the maximum stress of the CP and the plateau stress of the BCC. A considerable concurrence is observed between the peak stress exhibited by the CP and the stress level maintained at the plateau stage of the BCC (refer to Figure 6i). This convergence is particularly notable from approximately 10 to 48 per cent of the applied strain rate‡. The combination of the highest stresses arising from the CP and the BCC displays a superposition effect that seems to exhibit a similar pattern to the lowest stress levels in the BCC + CP composite structure, but this is not true for the BCC + CP structure itself. This conclusion is coincidental since this phenomenon does not occur when the CP is paired with the FCC, as shown by the results in Figure 6ii.

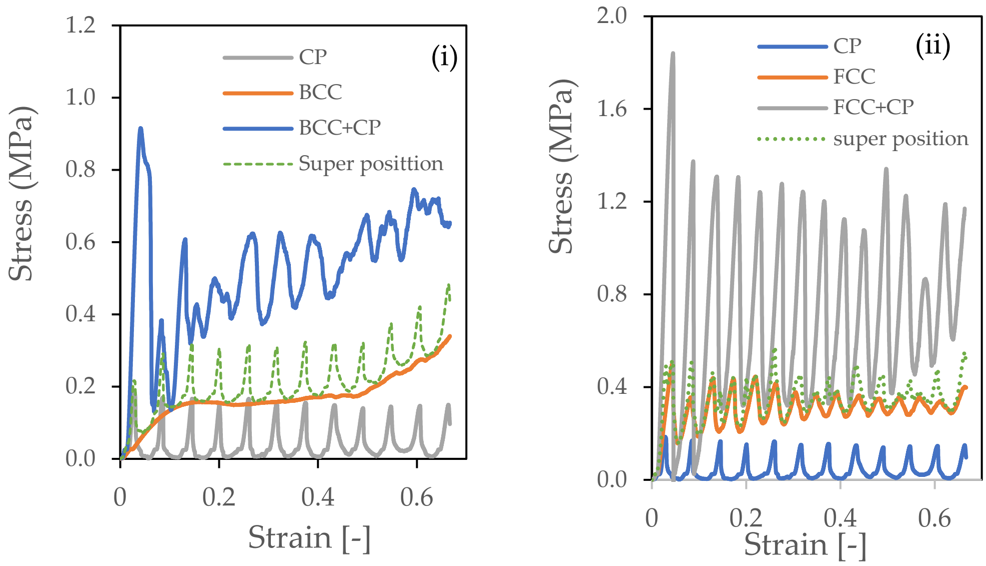


**Figure 6.** Stress-strain curves with the different lattice structures referencing with the CP structure. (**i**) superposition between CP and BCC does not equivalent with BCC + CP (**ii**) superposition between CP and FCC would not agree with FCC + CP; however, it clearly shows the agreement in rhythmic failure.

In contrast to CP, BCC, and BCC + CP, the concepts of superposition do not apply to FCC and FCC + CP. When introducing CP structure with FCC, a considerable enhancement in yield stress along the strain is possible. The maximum yield stress for FCC and FCC + CP are 357.4 ± 0.3 kPa and 1244.0 ± 1.6 kPa, respectively. Additionally, it appears that FCC may experience a somewhat quicker collapse in each layer than CP, although FCC and FCC + CP share the same collapsing strain precisely. Both FCC and FCC + CP exhibit higher initial stress compared to BCC and BCC + CP.

Another aspect that necessitates examination is the elastic modulus (E, Pa). The results of this study indicate a notable tendency for collapse that warrants attention, particularly with regards to the alterations observed in the elastic modulus of CP structures. Specifically, CP layers exhibited a remarkably similar elastic modulus, resulting in an insignificant variation of approximately 10.7 ± 0.2 MPa.‡. Although the outcomes did not exhibit a substantial response, they experienced a decrease of 63 per cent relative to the peak value of 16.07 ± 2.7 MPa. The elastic modulus of the BCC structure differed from that of the CP structure and other structures in the examined matrix. This is because the BCC structure was characterised by a bending-dominated structure that collapsed solely, rendering it unfeasible to observe the modulus series. Conversely, the other structure was stretching-dominated, meaning that the combination of BCC and CP might exhibit an indeterminate fluctuation in collapsing due to the arbitrary breaking of the studs.

Table 2 shows a response for the lattice structure with a solid sample. It is clearly seen that the lattice structures yield strength was not linearly reduced with the weight. The CP structure had maximum yield stress with no mean difference with the BCC structures‡ and these CP and BCC structures had the lowest yield stress in the test matrix. Compared to the reduction of yield stress with the weight saving, the CP was the lightest lattice structure, at approximately 94 per cent lighter than the solid, but it could withstand less than 1 per cent of the yield stress of solid. The BCC + CP and FCC + CP could benefit from their weight reduction as this reduction would increase yield stress more than twice. The most robust lattice structure was the FCC + CP sample, which had a weight saving of close to 15.8 per cent of the solid weight, but it performed better in terms of the relative stress at roughly 30 per cent.

**Table 2.** The mechanical properties of the different lattice structures.

| Structure | $\rho^*$ † [kg/m$^3$] | $\rho^*/\rho_S$ † [-]$\times10^{-2}$ | $\sigma^*$ † [kN/m$^3$] | $\sigma^*/\sigma_S$ †,⁂ [-]$\times10^{-2}$ | $E^*$ † [kN/m$^2$] | $E^*/E_S$ † [-]$\times10^{-2}$ |
|---|---|---|---|---|---|---|
| CP | 78.8 ± 0.6 $^a$ | 6.60 ± 0.05 $^a$ | 181.4 ± 0.1 $^a$ | 4.6 ± 0.3 $^a$ | 15.5 ± 4.3 $^b$ | 2.56 ± 0.73 $^b$ |
| BCC | 139.1 ± 2.8 $^b$ | 12.10 ± 0.24 $^b$ | 167.5 ± 0.1 $^a$ | 4.1 ± 0.8 $^a$ | 1.8 ± 0.5 $^a$ | 0.29 ± 0.08 $^a$ |
| FCC | 139.2 ± 9.1 $^b$ | 12.12 ± 0.79 $^b$ | 357.4 ± 0.3 $^b$ | 8.8 ± 2.7 $^b$ | 16.3 ± 3.0 $^b$ | 2.71 ± 0.50 $^b$ |
| BCC + CP | 155.8 ± 6.7 $^c$ | 13.6 ± 0.58 $^c$ | 938.8 ± 0.6 $^c$ | 23.2 ± 4.1 $^c$ | 40.5 ± 5.6 $^c$ | 6.72 ± 1.33 $^c$ |
| FCC + CP | 182.9 ± 8.2 $^d$ | 15.8 ± 0.71 $^d$ | 1244.0 ± 1.6 $^d$ | 30.7 ± 6.3 $^d$ | 53.8 ± 8.9 $^d$ | 8.92 ± 1.81 $^d$ |
| Solid | 1153.9 | 1 | 40,601.2 ± 5.2 | 1 | 600.8 | 1 |

Remark: † There is a significant reference difference at the 95 per cent confidence level; ⁂ This parameter offers a repeatability of less than 0.1 per cent; $^{a–d}$ show the subset order based on the post-hypothesis test.

As the stress property dramatically decreases, most lattices are carefully selected for suitable applications. From this test, it can be seen that the mechanical properties of the lattice structures were not able to compete with their original solid state except for the weight. Because all of the mechanical properties of the solid state were highly different from the lattice, those properties could be located in the outliner and had a discontinuous response; it would be better to track the data by normalising those solid properties.

All lattice structures can perform much better than a solid in an elastic modulus. For example, although the BCC is the weakest in stress, in this matrix, it can achieve excellence in an elastic modulus with a relative elastic modulus at 0.29 $^a$ per cent. Figure 7 represents an energy absorption per unit mass. Most of the force may transmitted to substrate in solid, thus its energy absorption was closely with FCC. Among these lattice structures, the highest energy absorption was the BCC + CP, then the FCC + CP. On the other hand, the lowest energy absorption was in the CP structure. The summation between the CP's energy absorption and either the BCC or FCC did not agree with the BCC + CP and FCC + CP. This is evidence to deny the concept of superposition within a lattice structure.

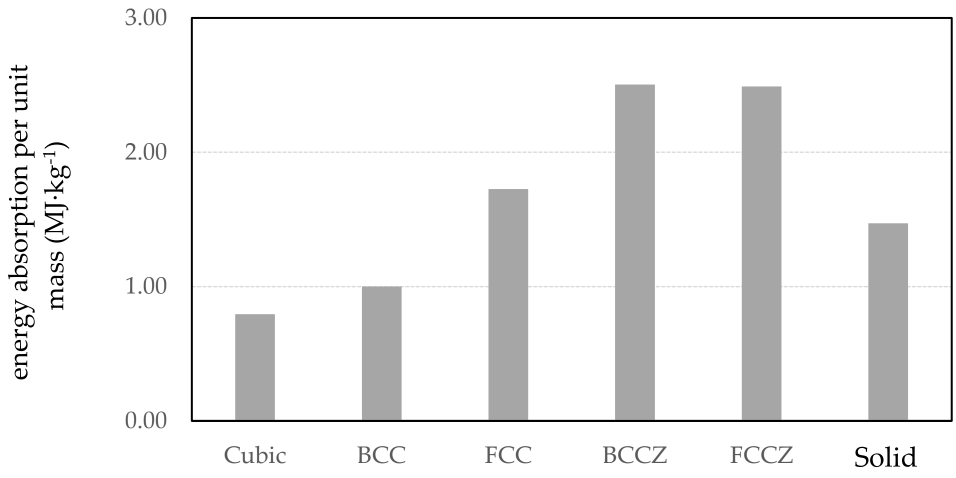


**Figure 7.** Energy absorption per unit mass of the lattice structures.

### 3.2. Empirical Modelling

The classical model of Gibson-Ashby [8,29] may be used to analyse these results. The outcomes of this investigation highlight a markedly pronounced contrast in properties between a solid and lattice. Specifically, this disparity is mainly exhibited in a normalised fashion about their solid properties ($x^*/x_s$). The empirical findings demonstrate that relative stress ($\sigma^*/\sigma_s$) and relative elastic modulus ($E^*/E_s$) were equally consistent. It is worth noting that the BCC + CP and FCC + CP topological configurations yielded a superior performance in both properties when compared to their respective primary structures (BCC and FCC) [27]. It can be seen that even though the relative density of the FCC + CP was twice that of the FCC relative density, and the elastic modulus of the FCC + CP was significantly increased by a factor of three.

After that, the plot between relative stress and the relative density provides analysis for all of the experimental data; this data reviled that there was a relative density between 0.10 and 0.15, and the stress of the lattice varied between about 0.005 and 0.039 times of the solid. As previously stated, the Gibson-Ashby model has the capability to prognosticate the fracture mode of the lacttice structures, which is apparent in references, particularly in the metallic lattice structures. However, this model may not be optimally suitable for the current outcome, as the associated density approaches the minimum limit of 0.003 Figure 8 shows the experimental results along with the Gibson-Ashby model [29], which The data indicates a weak correlation between the model and the experiment, with a correlation coefficient of 0.6 and a model correlation of 0.15. However, it is worth noting that the linear model appears to align with the experimental data. Although the model produced a satisfactory plot, the comparative stress of the CP differed from the other samples. To enhance the correlation coefficient, it is recommended to exclude the results of the CP sample. In relation to the relative elastic modulus, the Gibson-Ashby model for stretch dominance yielded a suboptimal correlation coefficient of 0.3. Nevertheless, it surprisingly presented the same connection between relative elastic modulus and relative density, also at 0.3 [22].

One thing that should be mentioned is that although the Gibson-Ashby [29] model is very famous and is accepted in the study of foam and lattice structures [8], as it was theoretically proven based on Euler's bulking [53]. However, if there are one or more structures, which have no significant difference in relative density (see Figure 8), it could lead to two or more response points at the same dependence variable, which would reduce an accurate model. For example, the relative density of the BCC and FCC samples are were insignificantly different with about 0.1; in this case, they show two different responses in the relative stress at approximately 0.005 and 0.010. Not only had CP a special collapse function, it did not agree with the other responses included relative stress and relative elastic modulus. That could be cause by the critical length of bucking column as mention on the literature [55,57]. This critical of any bucking column is limited by the boundary conditions: both ends fixed, both ends pinned, fixed and pinned, and fixed and free [55,57].

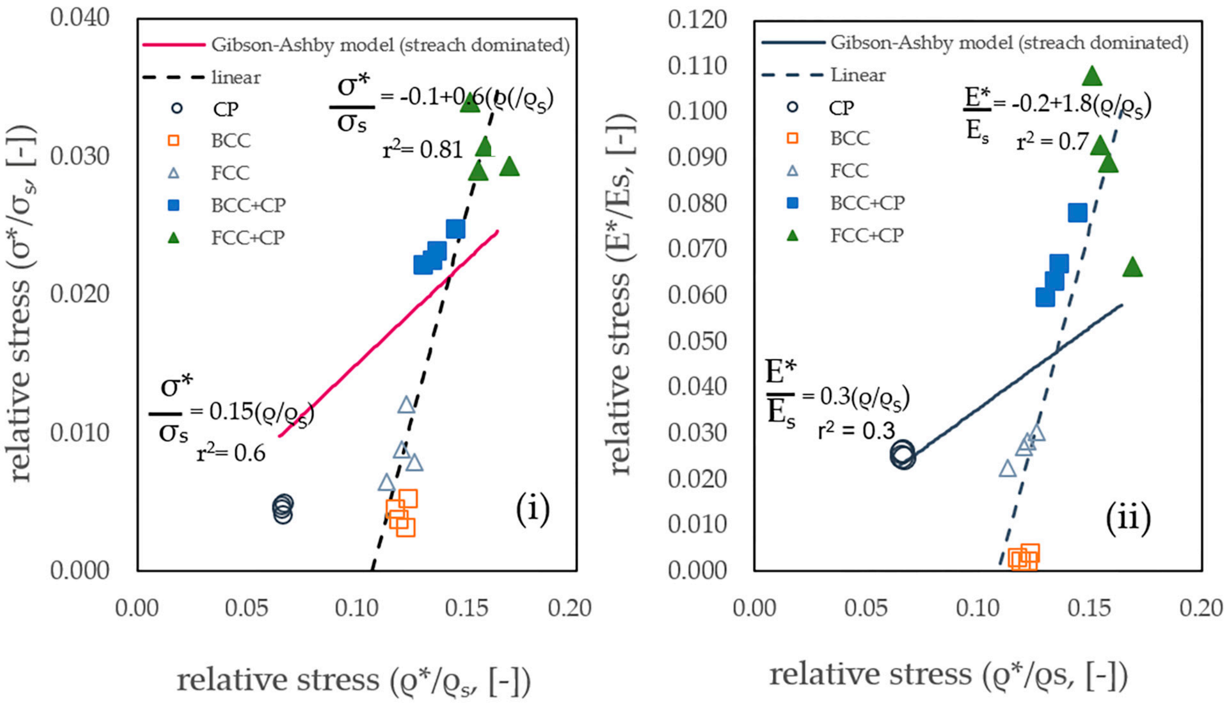


**Figure 8.** The plots of the empirical model are curve-fitting according to the Gibson-Ashby model and linear model (**i**) relative stress and (**ii**) relative elastic modulus.

### *3.3. Shock Impact Testing*

The lattice structures responded significantly with well-controlled pressure between 1 bar and 4 bars, equivalent to the force between 200 N and 320 N. According to Equation (1), the shock data in volts ($V_s$, V) were converted into acceleration (a, g) and then treated by a bandpass filter from MATLAB© 2019b with a manually adjusted baseline correction. The results from the impact testing adjusted the baseline, using a band-pass Butterworth filter with a fourth-order filter at 500 Hz. To avoid signal aliasing, the sampling rate was 512 $kS{\cdot}s^{-1}$, and the results of an impact in acceleration (a, g) obtained from Equation1 were converted to force and impulse by Equation (3).

The reference force is an experiment that can be performed by using the impact without installing any sample on the fingers of the test rig. It can be seen that the acceleration and force were narrow-based and had an extreme shape, with a shock at high frequency. The shock (force) was not only used as the reference input force but can also be used as the representative of a non-isolation system.

The first lattice structure is cubic perimeter (see Figure 9); under the impact force in cases (a)–(c). The acceleration results in "g" were 29.1 ± 0.9 g, 37.5 ± 0.1 g and 43.5 ± 0.1 g, respectively. This series of responses showed the convolution of the response signal or dispersion of the unmatching frequency, caused by two or more transverse waves travelling at different speeds. This dispersion effect of the force would be a benefit for using as in impact isolation with a low transmutability (T, [-]). However, it has a limitation as it can only take a compressive force of less than or equal to 289 ± 24 N.

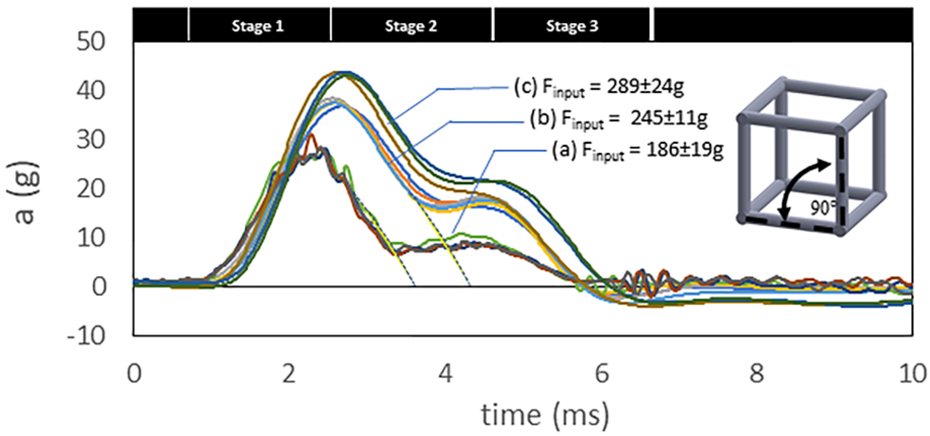


**Figure 9.** Shock acceleration response of a Cubic perimeter (CP) at the different input force levels ($F_{input}$) that are at (a) 186 ± 19 N (b) 245 ± 11 N (c) 289 ± 24 N. There is no experiment in case d at the $F_{input}$ 308 ± 11 N as the CP structure could not stand a force higher than level (c).

As mentioned earlier, the suggestion of using a cubic perimeter (CP) as the reference may rise in a quasi-static compression because this structure collapsed sequentially at the low strain rate, but under the shock acceleration, it could perform differently. The test results from this CP structure showed a sign of bending-dominated under all impulse input forces, especially at the higher impulse force. Under the quasi-static test, this structure did collapsed sequentially layer-by-layer but under a shock load, it was broken with a bending-dominated specimen. The series of impressions shown in Figure 10, from the beginning (i) to the end (iv); show the specimen was bending after impact (Figure 10iii). This phenomenon may be negative compared with a collapsing mode during the quasi-static part of the experiment.

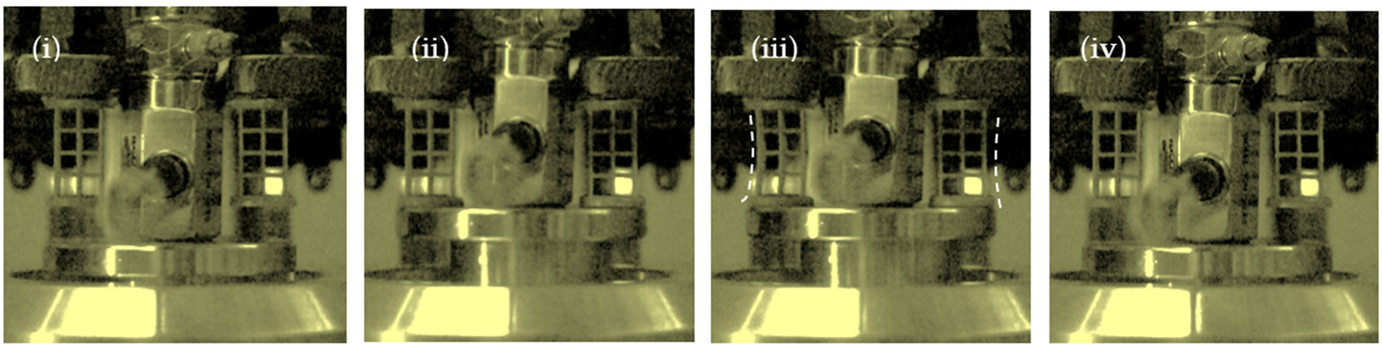


**Figure 10.** A series of impressions on the Cubic Perimeter (CP) under the shock excited force of 245 ± 11 N: (**i**) initial (**ii**) begin collision (**iii**) exhibited significant bending deformation (**iv**) end.

Therefore the series of specimens: CP, BCC, FCC, BCC + CP, FCC + CP and solid, was subjected to the four levels of shock impulse forces. The primary responses were the plots of unsteady acceleration (**a**, g) and impulse time (τ, ms). This impulse time can be estimated by an (Equation 4). Despite a sine function, the half-sine plot has another form in a cosine function that would be more convenient to use than a function of sine. The inversion of a response impulse multiplied by two is a response frequency (f, Hz).

Figure 11 shows the half-sine model plots against the experiment data under the excited force between 186 ± 19 N and 308 ± 11 N. It can be seen that the response impulse time was at a little lower level of excited force; hence, the higher the excited force is applied on the lattice structure, the higher response frequency would be, because of its impulse time reducing by 25 per cent between 186 ± 19 N and 308 ± 11 N.

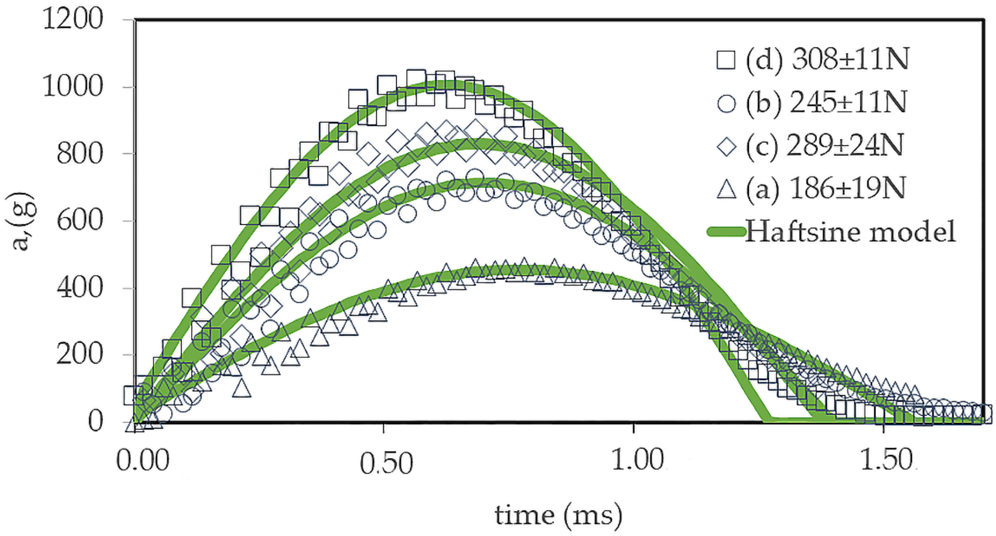


**Figure 11.** Half-sine pulse (solid line) over the shock (upto 1000 g) data at the different excited force between (**a**) 186 ± 19 N (**b**) 245 ± 11 N (**c**) 289 ± 24 N (**d**) 308 ± 11 N on the selected FCC + CP sample.

The excited impact force varied between 186 ± 19 N and 308 ± 11 N with five lattice structures and a solid. The test of responses suggested that the excited force was expected to influence these four responses$^{\dagger}$, and when the excited force increased, the response force, impulse and transmissibility were also increased$^{\dagger}$, while its impulse time obviously decreased† (see Table 3), Unlike an excited force, the type of structure or relative density may not offer the expected results. An increase in relative density positively affeced the force and transmissibility but could be negative for the impulse time†. The impulse response was surprisingly maximised at the 0.14 relative density in the BCC + CP structure.

**Table 3.** Mechanical responses of the different lattice structures.

| Structure | $\rho^*/\rho_S$ $^{\dagger}$ [-]$\times 10^{-2}$ | $F_{max}$ $^{\dagger}$ [N] | $\tau$ $^{\dagger}$ [ms] | P $^{\dagger}$ [N.ms] | T $^{\dagger}$ [-] |
|---|---|---|---|---|---|
| CP | 6.60 ± 0.05 [a] | 33.6 ± 0.3 [a] | 3.08 ± 0.03 [e] | 57.9 ± 0.9 [a] | 0.136 ± 0.001 [a] |
| BCC | 12.10 ± 0.24 [b] | 53.8 ± 0.9 [b] | 2.95 ± 0.03 [e] | 88.3 ± 0.7 [c] | 0.211 ± 0.002 [b] |
| FCC | 12.12 ± 0.79 [b] | 55.7 ± 0.9 [b] | 2.66 ± 0.01 [d] | 77.8 ± 1.0 [b] | 0.216 ± 0.001 [b] |
| BCC + CP | 13.6 ± 0.58 [c] | 62.8 ± 0.8 [c] | 2.41 ± 0.01 [c] | 91.2 ± 1.0 [c] | 0.238 ± 0.001 [c] |
| FCC + CP | 15.8 ± 0.71 [d] | 89.5 ± 1.0 [d] | 1.55 ± 0.01 [b] | 80.1 ± 0.8 [b] | 0.341 ± 0.002 [d] |
| Solid | 1 | 102.2 e | 1.05 [a] | 53.6 [a] | 0.38 [e] |

Remark: $^{\dagger}$ There is a significant reference difference at the 95% confidence level. [a–e] show the subset order based on the post-hypothesis test.

Moreover, the interaction between these fixed factors also had a large effect on all of the responses. The peaks of the response forces were accurately varied with a narrow band of measurement uncertainty at less than 2 per cent. Table 3 shows the depended variables that are on one fixed factor that is relative density. The other fix factor was the excited force. Amongst these responses, the most accurate responses was an impulse time that is measurable with a repeatability of less than 1 per cent. It was observed that the FCC + CP was withstanding at the higher shock pulse level among all of the lattice structures (see Table 3). That would be great for a structural application because this structure was stiffer and more than the other structures. The impulse (**P**, N·s) can be estimated by integrating the total area under the response curves, which would not be the product between F and $\tau$. In theory, this impulse could be roughly the same with a similar structure at the same level of an excited force; thus, the repeatability of the impulse response would be less than 2 per cent.

The result from Table 3 ($F_{max}$) shows no significant difference between the BCC and FCC at the 95% confidence level. However, the interactions between the relative density and excited force also significantly differed on impulse and maximised at 0.14 the relative density (or BCC + CP). From the force's evolution, it can be seen that the area under the curve of the BCC + CP was the biggest. From this experiment, the possible shock responses in lattice structure were from the FCC + CP $^{a}$, BCC + CP $^{b}$, BCC $^{c}$, FCC $^{c}$ and CP $^{d}$, respectively. There was no mean difference between the BCC$^{c}$ and FCC$^{c}$ at the same confidence level denoted by "C". Thus, this could lead to the impulse difference from the maximum force graph. Even though the maximum force of these two samples would not have any mean difference between the group, as the data from the FCC were only between 186 ± 19 N and 289 ± 24 N.

Even if responses of BCC and BCC + CP have a significant different in maximum transmitting force, it found that the impulse responses were sparingly the same at the homogenous scale "c". Thus, impulse responses of these structures may independent on their relative density but it would depend on the architecture of their structures. When an input force increases, the maximum force will nonlinearly increase (see Figure 12). Moreover, the maximised energy absorption structure was the BCC + CP (see Figure 7) with not to fluctuate of stress over the changing of strain that could highlighted the BCC + CP as a good candidate for use in isolation application.

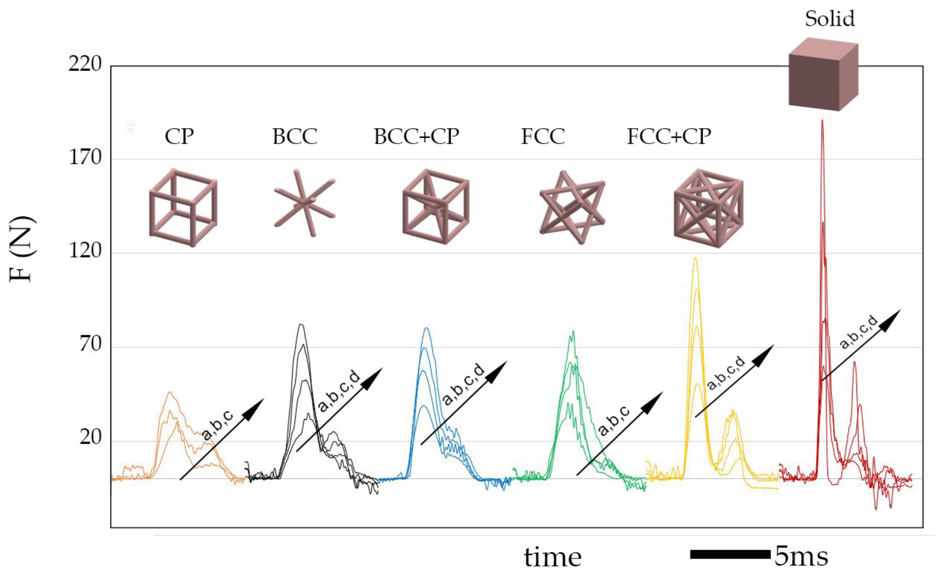


**Figure 12.** The evolution of the shock response at the four levels of excited forces: (**a**) 186 ± 19 N, (**b**) 245 ± 11 N, (**c**) 289 ± 24 N and (**d**) 308 ± 11 N).

The impulse frequency (f, Hz) can be estimated from the inversion of twice the impulse time ($1/(2{\cdot}\tau)$). This frequency was a linear function of excited force and mainly had the same trend with the maximum force; hence, all the impulse responses increased linearly with excited force, and depended on the rigidity of the lattice structure, and as the more rigid structures, it could lead to a higher frequency. The impulse frequency of most of the lattices varied roughly between 140–350 Hz (see Figure 13iii). Although, these frequencies may two time changing, the convolution curve may happen roughly at 5 ms.

The parameter that denotes the ability to propagate a force, known as transmissibility (T), is calculated by dividing the maximum force (Fmax) by the input force (Finput). Under low levels of excited force, the FCC + CP lattice structure exhibited similarity to a solid material, but its performance was inferior to that of the solid structure, particularly when subjected to high input forces exceeding 300 N. At this magnitude of force, the transmissibility of the FCC + CP lattice structure was reduced by 60% compared to the solid material, but enhanced by 50% when compared to the BCC + CP lattice structure.

All lattice structures demonstrated potential for use in compression isolation and their frequency responses were dependent on their respective structures. (see Figure 13iv).

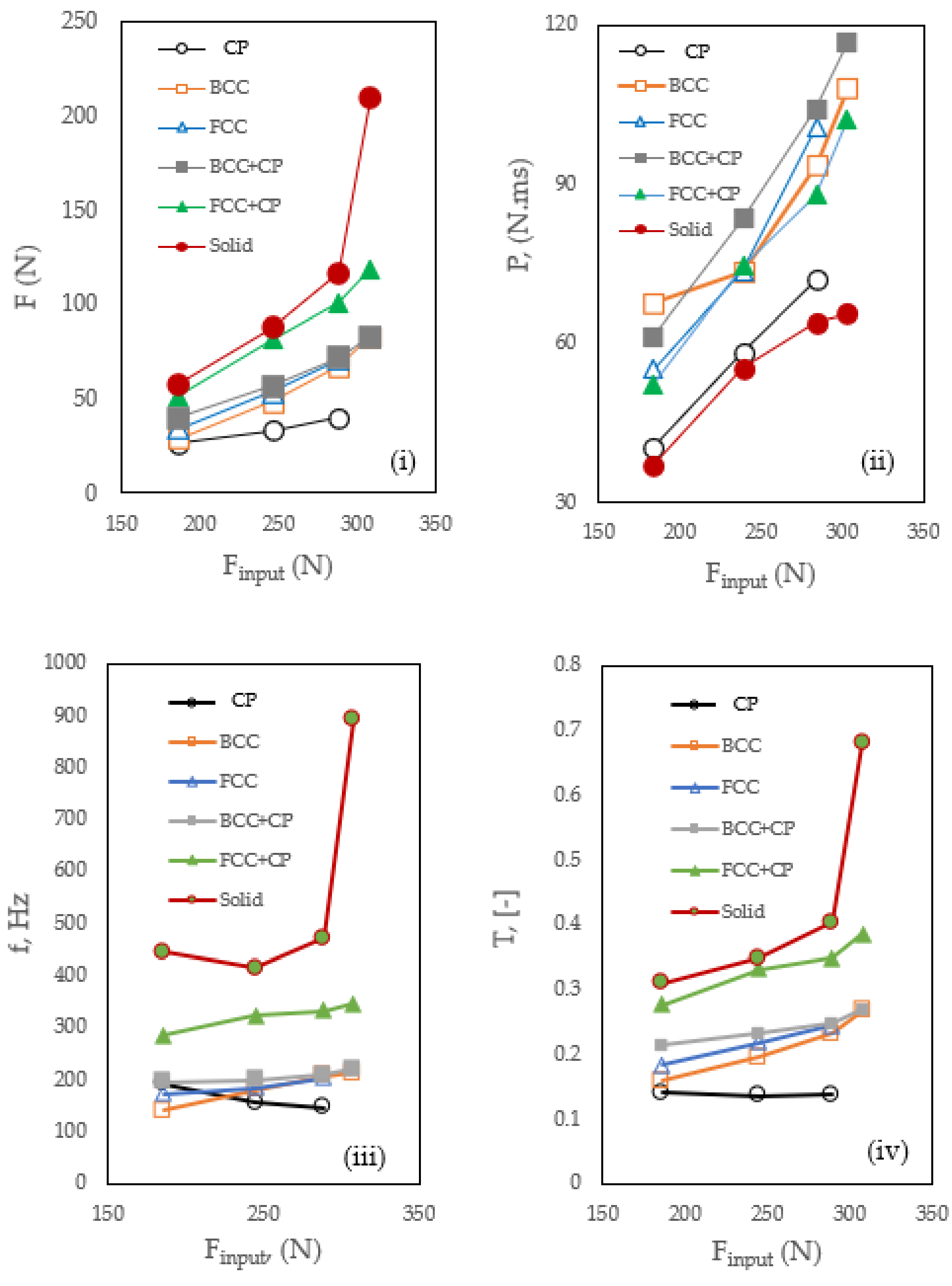


**Figure 13.** The effect of maximum input force over (**i**) response force (**ii**) impulse (**iii**) response frequency and (**iv**) transmissibility at the different input forces with the different lattices.

Based on the collected experimental data, it was observed that there existed a correlation between the rate of deformation and the difference in momentum or impulse resulting from the applied force, which in turn generated potential energy and incurred losses due to the viscous-elastic effect. The magnitude of the input force was directly proportional to the kinetic energy imparted by the impactor. Following the impact with the central point (CP), a portion of the force was transferred to the underlying substrate and the lattice structure, causing an initial elongation of the curtain length, and subsequently leading to a relaxation mode of the viscous-elastic material.

The lattice structure has the potential to reduce the shock force. The findings not only encompassed the outcome of the quasi-static examination but also contributed to the results of an experiment stimulated by pneumatic shock, capable of generating high acceleration with minimal impulse force. The entirety of the experimental outcomes indicate that the lattice structure may have the potential to alleviate the impact of shock. Table 3 indicates that the homogenous characteristic of relative density was similar to the response forces. However, it is important to note that the main impulse time may depend on the architecture of the lattice structure, as indicated by the 10 per cent offset of the haft-sine plot from its baseline (see Figures 11 and 12). Although the convolution curve of all lattice structures demonstrated very similar responses in time, at roughly 5 ms, the main impulse time may vary depending on the architecture of the lattice structure. Figure 13iii showed the separated effect between excited force and architecture and suggested that the impulse time (inversion of frequency) may be significantly reduced with an excited force above 290 N in solid, but it slightly decreased with excited force, particularly with high relative density, such as the FCC + CP structure. Using a lattice structure may benefit in reducing transmissibility, as demonstrated in Figure 13iv. This effect was found to be particularly strong at high levels of excited force. The impulse shows in Table 3 with Figure 13ii is a product of impulse time with the force that is independent of relative density but it depends on the architect of those lattice structures.

## 4. Conclusions

The use of lattice structures has gained considerable popularity in various applications due to their advantageous weight-to-stress ratio. However, the choice of lattice structure must be carefully considered in accordance with the specific requirements of each application. This study focuses on the examination of three fundamental lattice structures cubic perimeter (CP), body face centered cubic (BCC), and face centered cubic (FCC) and the reinforcement structures created by combining these basic structures with a CP structure: BCC + CP and FCC + CP. These five structures and solid were fabricated by a photopolymer printer.

In this investigation, the collapsing mode and stress-strain relationships were analysed using quasi-static testing with a cohort of experimental data. The results indicated that most of the lattice structures failed in a stretching-dominated mode, but the BCC failure mode was bending-dominated. The bending mode failure in the BCC was a result of stress distribution patterns as the two opposite pyramids joined at the peaks. The failure mode of the close-packed structure was also classified as stretching-dominated; however, it was assigned the particular category of sequential layer-by-layer collapse mode due to the high incidence of stress along the vertical columns and a more diluted stress distribution along the horizontal connections of each cell. The other structures were collapsed with stretching dominated.

Under the quasi-static test, the null hypotheses were established as there were not any differences between the mechanical responses (relative density, relative stress and relative elastic modulus) with different lattice structures at a 95 per cent confidence level. Not only were all of the null hypotheses rejected with highly significant difference levels, but most of the responses mainly depended on the lattice structures; however, homogeneous results established that there was no significant difference in the relative density of the BCC and FCC. Therefore, the estimated weight of the BCC and FCC might not be statistically different, but they did not offer the same stress and strain because their architecture did not show identical responses at the specific compressive force, and one of the obvious results was different failure modes happening between these two structures, which resulted in the difference in relative stress and relative elastic modulus. Thus, this can result in inaccurate of the empirical model. It seems that most of the relative stress and relative elastic increased linearly with an increase of relative density, but there were exceptions with the CP and BCC. Under a quasi-stress test, the highest stress response was the FCC + CP, the strongest structure, with the smallest being the elastic modulus of the BCC, which was bending-dominated.

A shock impulse test of closely 300 N (upto 1000 g) offered a clear picture of the differences between the lattice structures. The solid structure was obviously the strongest structure as it had a high rigidity; hence, it would be great to use in structural applications, but the lattice structure was lighter, with the highest shock absorption. In the case of the FCC + CP structure, there was an average shock force deduction of approximately 20 per cent, however this structure could save weight by roughly 85 per cent compared with the solid structure. Moreover, the average lighter weight of a lattice structure would be better operated if there was any significant difference in the shock impulse time in the same lattice structures, which can yield less difference in operating frequency. The other advantages of lattice structures were their shock compression insolation properties. It can be seen that solid structures had the poorest shock insolation properties as it had the highest transmissibility compared to the lattice structures. The impulse of the BCC + CP was the highest and this showed that the momentum change of the collision in this sample was the maximum. Also, this BCC + CP has nearly identical shock impulse with BCC. In summary, our results tentatively suggest that the body-centered cubic with cubic perimeter (BCC + CP) structure may be a suitable option for shock isolation applications, such as safety gear as mentioned earlier. However, further optimization of the BCC + CP structure through simulation and other testing methods may be necessary to fully realize its potential for practical applications. In addition, the other lattice structures may or may not be suitable for individual use, but could potentially be used as complementary structures to enhance the mechanical properties of individual parts in order to achieve their specific objectives.

**Author Contributions:** P.D.: Investigation, Data curation, Writing—Original draft preparation; T.J.: Supervision; K.J.: Conceptualisation, Methodology, Supervision, Writing—Reviewing and Editing. All authors have read and agreed to the published version of the manuscript.

**Funding:** This research received no external funding.

**Institutional Review Board Statement:** Not applicable.

**Informed Consent Statement:** Not applicable.

**Data Availability Statement:** The raw data required to reproduce these findings cannot be shared at this time as the data also forms part of an ongoing study; however, analysis data for Figures 6–8 and 11 are repository at https://data.mendeley.com/datasets/fhv5y4tzgc/1 (accessed on 7 May 2023).

**Acknowledgments:** This work would not have been possible without financial support from the Faculty of Engineering, Thammasat University. Finally, the authors would like to express our gratitude to the Electricity Generating Authority of Thailand for giving permission to use the shock rigs.

**Conflicts of Interest:** The authors declare no conflict of interest.

## References

1. Wang, B.; Wu, L.-Z.; Ma, L.; Feng, J.-C. Low-velocity impact characteristics and residual tensile strength of carbon fiber composite lattice core sandwich structures. *Compos. Part B Eng.* **2011**, *42*, 891–897. [CrossRef]
2. Karthick, B.; Balaji, S.; Maniiarasan, P. Structural Analysis of Fuselage with Lattice Structure. *Int. J. Eng. Res.* **2013**, *2*, 1909–1913.
3. Matlack, K.H.; Bauhofer, A.; Krödel, S.; Palermo, A.; Daraio, C. Composite 3D-printed metastructures for low-frequency and broadband vibration absorption. *Proc. Natl. Acad. Sci. USA* **2016**, *113*, 8386–8390. [CrossRef] [PubMed]
4. Kang, D.-S.; Park, S.-H.; Son, Y.; Yeon, S.-M.; Kim, S.H.; Kim, I.-Y. Multi-lattice inner structures for high-strength and light-weight in metal selective laser melting process. *Mater. Des.* **2019**, *175*, 107786. [CrossRef]
5. Chang, Y.-Y.; Amrutwar, S. Effect of Plasma Nitriding Pretreatment on the Mechanical Properties of AlCrSiN-Coated Tool Steels. *Materials* **2019**, *12*, 795. [CrossRef] [PubMed]
6. Compton, B.G.; Lewis, J.A. 3D-Printing of Lightweight Cellular Composites. *Adv. Mater.* **2014**, *26*, 5930–5935. [CrossRef] [PubMed]
7. Pan, C.; Han, Y.; Lu, J. Design and Optimization of Lattice Structures: A Review. *Appl. Sci.* **2020**, *10*, 6374. [CrossRef]
8. Gibson, L.J.; Ashby, M.F. *Cellular Solids: Structure and Properties*, 2nd ed.; Cambridge University Press: Cambridge, UK, 1997. Available online: https://www.cambridge.org/core/books/cellular-solids/BC25789552BAA8E3CAD5E1D105612AB5 (accessed on 21 January 2023). ISBN 9780521499118.
9. Xue, B.; Peng, Y.-X.; Ren, S.-F.; Liu, N.-N.; Zhang, Q. Investigation of impact resistance performance of pyramid lattice sandwich structure based on SPH-FEM. *Compos. Struct.* **2021**, *261*, 113561. [CrossRef]

10. Ashab, A.A.; Ruan, D.; Lu, G.; Bhuiyan, A.A. Finite Element Analysis of Aluminum Honeycombs Subjected to Dynamic Indentation and Compression Loads. *Materials* **2016**, *9*, 162. [CrossRef]
11. Schrodt, M.; Benderoth, G.; Kühhorn, A.; Silber, G. Hyperelastic description of polymer soft foams at finite deformations. *Tech. Mech.* **2005**, *25*, 162–173.
12. Fu, T.; Chen, Z.; Yu, D.; Wang, X.; Lu, W. Sound transmission from stiffened double laminated composite plates. *Wave Motion* **2017**, *72*, 331–341. [CrossRef]
13. Fu, T.; Chen, Z.; Yu, H.; Zhu, X.; Zhao, Y. Sound transmission loss behavior of sandwich panel with different truss cores under external mean airflow. *Aerosp. Sci. Technol.* **2019**, *86*, 714–723. [CrossRef]
14. Gao, H.; Jin, X.; Yang, J.; Zhang, D.; Zhang, S.; Zhang, F.; Chen, H. Porous structure and compressive failure mechanism of additively manufactured cubic-lattice tantalum scaffolds. *Mater. Today Adv.* **2021**, *12*, 100183. [CrossRef]
15. Wally, Z.J.; Van Grunsven, W.; Claeyssens, F.; Goodall, R.; Reilly, G.C. Porous Titanium for Dental Implant Applications. *Metals* **2015**, *5*, 1902–1920. [CrossRef]
16. Leary, M.; Mazur, M.; Williams, H.; Yang, E.; Alghamdi, A.; Lozanovski, B.; Zhang, X.; Shidid, D.; Farahbod-Sternahl, L.; Witt, G.; et al. Inconel 625 lattice structures manufactured by selective laser melting (SLM): Mechanical properties, deformation and failure modes. *Mater. Des.* **2018**, *157*, 179–199. [CrossRef]
17. Keni, L.G.; Singh, V.; Singh, N.; Thyagi, A.; Kalburgi, S.; Chethan, N. Conceptual design and analysis of a car bumper using finite element method. *Cogent Eng.* **2021**, *8*, 1976480. [CrossRef]
18. Federal Motor Vehicle Safety Standards; Occupant Crash Protection. Title 49 of the Code of Federal Regulations (CFR), Part 571.208. Available online: https://www.nhtsa.gov/sites/nhtsa.gov/files/nprm_208_0.pdf (accessed on 21 January 2023).
19. The Society of Automotive Engineers. *SAE J211-1: Instrumentation for Impact Test*; SAE International: Warrendale, PA, USA, 2022. Available online: https://www.sae.org/standards/content/j211/1_202208 (accessed on 21 January 2023).
20. The, U.S. Consumer Product Safety Commission, Part 1203 Safety Standard for Bicycle Helmets. Available online: https://www.law.cornell.edu/cfr/text/16/part-1203 (accessed on 21 January 2023).
21. Yang, Y.; Shan, M.; Zhao, L.; Qi, D.; Zhang, J. Multiple strut-deformation patterns based analytical elastic modulus of sandwich BCC lattices. *Mater. Des.* **2019**, *181*, 107916. [CrossRef]
22. Alomar, Z.; Concli, F. Compressive behavior assessment of a newly developed circular cell-based lattice structure. *Mater. Des.* **2021**, *205*, 109716. [CrossRef]
23. Zhang, H.; Wang, X.; Shi, Z.; Xue, J.; Han, F. Compressive and Energy Absorption Properties of Pyramidal Lattice Structures by Various Preparation Methods. *Materials* **2021**, *14*, 6484. [CrossRef]
24. Ling, C.; Cernicchi, A.; Gilchrist, M.D.; Cardiff, P. Mechanical behaviour of additively-manufactured polymeric octet-truss lattice structures under quasi-static and dynamic compressive loading. *Mater. Des.* **2019**, *162*, 106–118. [CrossRef]
25. Dar, U.A.; Mian, H.H.; Abid, M.; Topa, A.; Sheikh, M.Z.; Bilal, M. Experimental and numerical investigation of compressive behavior of lattice structures manufactured through projection micro stereolithography. *Mater. Today Commun.* **2020**, *25*, 101563. [CrossRef]
26. Chen, X.; Ji, Q.; Wei, J.; Tan, H.; Yu, J.; Zhang, P.; Laude, V.; Kadic, M. Light-weight shell-lattice metamaterials for mechanical shock absorption. *Int. J. Mech. Sci.* **2020**, *169*, 105288. [CrossRef]
27. Sangle, S.D. *Design and Testing of Scalable 3D-Printed Cellular Structures Optimised for Energy Absorption*; Wright State University: Dayton, OH, USA, 2017. Available online: https://corescholar.libraries.wright.edu/etd_all/1731 (accessed on 21 January 2023).
28. Tancogne-Dejean, T.; Li, X.; Diamantopoulou, M.; Roth, C.C.; Mohr, D. High Strain Rate Response of Additively-Manufactured Plate-Lattices: Experiments and Modeling. *J. Dyn. Behav. Mater.* **2019**, *5*, 361–375. [CrossRef]
29. Gibson, L.J.; Ashby, M.F. The Mechanics of Three-Dimensional Cellular Materials. *Proc. R. Soc. Lond. A Math. Phys. Sci.* **1982**, *382*, 43–59. [CrossRef]
30. Hunt, G.W.; Peletier, M.A.; Wadee, M. The Maxwell stability criterion in pseudo-energy models of kink banding. *J. Struct. Geol.* **1999**, *22*, 669–681. [CrossRef]
31. Zhao, S.; Zong, X.; Wu, N. Design of Load Path-oriented BCCz Lattice Sandwich Structures. In *Journal of Physics: Conference Series*; IOP Publishing: Bristol, UK, 2022. [CrossRef]
32. Robert, D. *Accelerometer Shock Sensitivity Calibration Using a Pneumatic Exciter*; PCB Piezotronics, Inc.: Depew, NY, USA, 2016. Available online: https://www.pcb.com/contentstore/MktgContent/WhitePapers/WPL_38_Accelerometer_Shock_Sensitivity_Calibration.pdf (accessed on 21 January 2023).
33. Prangphanta, S.; Sukchoksirichaiporn, K.; Doungkum, P.; Jearsiripongkul, T.; Panyadilok, S.; Tongkum, A.; Jiamjiroch, K. A Preliminary Study of Shock Calibration Machine for Accelerometer Calibration. In Proceedings of the 5th International Conference on Mechanical, System and Control Engineering, Lecture Notes in Mechanical Engineering, Kazan, Russia, 28–30 May 2021; Lei, X., Koryanov, V.V., Eds.; Springer: Singapore, 2022; pp. 225–232. [CrossRef]
34. *ISO 16063-22:2005*; Methods for the Calibration of Vibration and Shock Transducers—Part 22: Shock Calibration by Comparison to a Reference Transducer. International Standard Organisation: Geneva, Switzerland, 2015. Available online: https://www.iso.org/standard/32051.html (accessed on 21 January 2023).
35. Vrana, R.; Koutny, D.; Paloušek, D. Impact resistance of different types of lattice structures manufactured by SLM. *MM Sci. J.* **2016**, *2016*, 1579–1585. [CrossRef]

36. Foster, J.; Frew, D.; Forrestal, M.; Nishida, E.; Chen, W. Shock testing accelerometers with a Hopkinson pressure bar. *Int. J. Impact Eng.* **2012**, *46*, 56–61. [CrossRef]
37. Nozato, H.; Usuda, T.; Ota, A.; Ishigami, T.; Kudo, K. Development of Shock Acceleration Calibration Machine in NMIJ. In Proceedings of the TC22 International Conference Cultivating Metrological Knowledge, Merida, Mexico, 27–30 November 2007.
38. Fíla, T.; Koudelka, P.; Falta, J.; Zlámal, P.; Rada, V.; Adorna, M.; Bronder, S.; Jiroušek, O. Dynamic impact testing of cellular solids and lattice structures: Application of two-sided direct impact Hopkinson bar. *Int. J. Impact Eng.* **2021**, *148*, 103767. [CrossRef]
39. Bourne, N.K. On the Shock Response of Polymers to Extreme Loading. *J. Dyn. Behav. Mater.* **2016**, *2*, 33–42. [CrossRef]
40. Bourne, N.K.; Millett, J.C.F. The high-rate response of an elastomer. *Proc. R. Soc. A Math. Phys. Eng. Sci.* **2003**, *459*, 567–576. [CrossRef]
41. Jhou, S.-Y.; Hsu, C.-C.; Yeh, J.-C. The Dynamic Impact Response of 3D-Printed Polymeric Sandwich Structures with Lattice Cores: Numerical and Experimental Investigation. *Polymers* **2021**, *13*, 4032. [CrossRef] [PubMed]
42. Weeks, J. Mechanical Response of Lattice Structures under High Strain-Rate and Shock Loading. Doctoral Dissertation, California Institute of Technology, Pasadena, CA, USA, 2022. [CrossRef]
43. Mantovani, S.; Giacalone, M.; Merulla, A.; Bassoli, E.; Defanti, S. Effective Mechanical Properties of AlSi7Mg Additively Manufactured Cubic Lattice Structures. *3D Print. Addit. Manuf.* **2022**, *9*, 326–336. [CrossRef]
44. Elmadih, W. Additively Manufactured Lattice Structures for Vibration Attenuation. Ph.D. Thesis, The University of Nottingham, Nottingham, UK, 2019.
45. The International Organisation Established by the Metre Convention. Guide to the Expression of Uncertainty in Measurement. In *Evaluation of Measurement Data*, 1st ed.; Joint Committee for Guides in Metrology (JCGM): Kentfield, CA, USA, 2008. Available online: https://www.bipm.org/documents/20126/2071204/JCGM_100_2008_E.pdf/cb0ef43f-baa5-11cf-3f85-4dcd86f77bd6 (accessed on 21 January 2023).
46. *ISO/ASTM 52900*; Additive Manufacturing General Principles Terminology. International Organization for Standardization (ISO): Geneva, Switzerland, 2015. Available online: https://www.iso.org/standard/69669.html (accessed on 21 January 2023).
47. Austermann, J.; Redmann, A.J.; Dahmen, V.; Quintanilla, A.L.; Mecham, S.J.; Osswald, T.A. Fiber-Reinforced Composite Sandwich Structures by Co-Curing with Additive Manufactured Epoxy Lattices. *J. Compos. Sci.* **2019**, *3*, 53. [CrossRef]
48. *ASTM D1621-16*; Standard Test Method for Compressive Properties of Rigid Cellular Plastics. American Society for Testing and Materials: West Conshohocken, PA, USA, 2015. Available online: https://www.astm.org/d1621-16.html (accessed on 21 January 2023).
49. Cingesar, I.K.; Marković, M.-P.; Vrsaljko, D. Effect of post-processing conditions on polyacrylate materials used in stereolithography. *Addit. Manuf.* **2022**, *55*, 102813. [CrossRef]
50. R Core Team. *R: A Language and Environment for Statistical Computing*; R Foundation for Statistical Computing: Vienna, Austria, 2022. Available online: https://www.r-project.org (accessed on 21 January 2023).
51. Inchausti, P. *Statistical Modeling with R: A Dual Frequentist and Bayesian Approach for Life Scientists*; Oxford University Press: Oxford, UK, 2022; ISBN 9780192859013. [CrossRef]
52. *ASTM D695-02*; Standard Test Method for Compressive Properties of Rigid Plastics. International Organization for Standardization (ISO): West Conshohocken, PA, USA, 2002. [CrossRef]
53. Gibson, L.J. The Elastic and Plastic Behaviour of Cellular Materials. Doctoral Dissertation, Cambridge University, Cambridge, UK, 1981. [CrossRef]
54. Jiamjiroch, K.; Jearsiripongkul, T.; Bunnjaweht, D.; Doungkum, P.; Panyadilok, S.; Tongkum, A. A Design and Development of a Pneumatic Shock Calibration Machine. In Proceedings of the 2023 Third International Symposium on Instrumentation, Control, Artificial Intelligence, and Robotics (ICA-SYMP), Bangkok, Thailand, 18–20 January 2023; pp. 33–36.
55. Alghamdi, A.; Leary, M.; Qian, M.; Xu, W.; Brandt, M. Critical Buckling Load for Lattice Column Elements with Variable Dimensions. In Proceedings of the International Conference on Design and Technology, Austin, TX, USA, 23–25 May 2017; Collins, P.K., Ed.; KnE Publishing: Dubai, United Arab Emirates, 2017; pp. 84–90. [CrossRef]
56. Park, K.-M.; Min, K.-S.; Roh, Y.-S. Design Optimization of Lattice Structures under Compression: Study of Unit Cell Types and Cell Arrangements. *Materials* **2022**, *15*, 97. [CrossRef] [PubMed]
57. Gardner, L.A.; Nethercot, D.A.; Gulvanessian, H. Designers' Guide to EN 1993-1-1 Eurocode 3: Design of Steel Structures. 1993. Available online: https://www.icevirtuallibrary.com/doi/abs/10.1680/dgte3.31630 (accessed on 21 January 2023).


**Disclaimer/Publisher's Note:** The statements, opinions and data contained in all publications are solely those of the individual author(s) and contributor(s) and not of MDPI and/or the editor(s). MDPI and/or the editor(s) disclaim responsibility for any injury to people or property resulting from any ideas, methods, instructions or products referred to in the content.